6-20-2007

Optically Thick [O I] and [C II] Emission toward NGC 6334A

N. P. Abel
University of Cincinnati

A. P. Sarma
Depaul University

Thomas H. Troland
University of Kentucky, troland@pa.uky.edu

Gary J. Ferland
University of Kentucky, gary@uky.edu

Optically Thick [O I] and [C II] Emission toward NGC 6334A

Digital Object Identifier (DOI)
http://dx.doi.org/10.1086/517987

The Astrophysical Journal, 662:1024–1032, 2007 June 20

OPTICALLY THICK [O I] AND [C II] EMISSION TOWARD NGC 6334A

N. P. Abel,[1] A. P. Sarma,[2] T. H. Troland,[3] and G. J. Ferland[3]

Received 2006 November 14; accepted 2007 February 9

ABSTRACT

This work focuses on [O I] and [C II] emission toward NGC 6334A, an embedded H^+ region/PDR only observable at infrared or longer wavelengths. A geometry in which nearly all the emission escapes out the side of the cloud facing the stars, such as Orion, is not applicable to this region. Instead, we find the geometry to be one in which the H^+ region and associated PDR is embedded in the molecular cloud. Constant-density PDR calculations are presented which predict line intensities as a function of A_V [or $N(H)$], hydrogen density (n_H), and incident UV radiation field (G_0). We find that a single-component model with $A_V \sim 650$ mag, $n_H = 5 \times 10^5$ cm^{-3}, and $G_0 = 7 \times 10^4$ reproduces the observed [O I] and [C II] intensities, and that the low [O I] 63 to 146 μm ratio is due to line optical depth effects in the [O I] lines, produced by a large column density of atomic/molecular gas. We find that the effects of a density law would increase our derived A_V, while the effects of an asymmetric geometry would decrease A_V, with the two effects largely canceling. We conclude that optically selected H^+ regions adjacent to PDRs, such as Orion, likely have a different viewing angle or geometry than similar regions detected through IR observations. Overall, the theoretical calculations presented in this work have utility for any PDR embedded in a molecular cloud.

Subject headings: dust, extinction — infrared: general — line: formation — radiative transfer

1. INTRODUCTION

Photodissociation regions or photon-dominated regions (PDRs) mark the transition from ionized to atomic and molecular gas in star-forming regions. PDRs are usually physically adjacent to H II regions (which we refer to as H^+ regions in this work), although environments such as reflection nebulae (Hollenbach & Tielens 1997; Young Owl et al. 2002) and much of the diffuse interstellar medium (ISM), which are exposed to few hydrogen-ionizing photons, also contain PDRs. Overall, the bulk of mass in star-forming environments is contained in PDRs, and so these regions allow us to study important physical processes in astrophysical environments, such as grain physics, molecular formation, and the interplay between magnetic, thermal, turbulent, and gravitational energies (Hollenbach & Tielens 1997; Crutcher 1999).

In this paper, we focus our attention on a region where the assumed geometry used in most PDR calculations (e.g., Tielens & Hollenbach 1985a, 1985b; Kaufman et al. 1999) fails to reproduce the [O I] emission-line fluxes at 63 and 146 μm and [C II] 158 μm emission. In § 2 we review the PDR diagnostic capabilities of [O I] and [C II] emission. Section 3 summarizes the observational data for NGC 6334A. Section 4 gives the details of our theoretical calculations. Section 5 gives our results, and § 6 gives our conclusions.

2. [O I] AND [C II] EMISSION AS A PDR DIAGNOSTIC

2.1. *Background*

Since their first detection ([O I] $^3P_1 \rightarrow {}^3P_2$, Melnick et al. 1979; [O I] 146 μm $^3P_0 \rightarrow {}^3P_1$, Stacey et al. 1983; [C II] 158 μm $^2P_{3/2} \rightarrow {}^2P_{1/2}$, Russell et al. 1980; all in Orion), emission from [O I] and [C II] has been widely regarded as coming from PDRs because of two reasons. One is that the ionization potentials of O^0 and C^0 mean that O^0 and C^+ are the dominant stages of ionization beyond the H^+ ionization front. The second reason is that the excitation energies for [O I] and [C II] emission range from 92–330 K, which are also the characteristic temperatures found in PDRs. Therefore, these transitions are easily excited by collisions with H and H_2.

Theoretical calculations have shown the diagnostic utility of [O I] and [C II] emission in many regions (Tielens & Hollenbach 1985a, 1985b). Such calculations involve combining current theories of atomic, molecular, and grain processes in PDRs with solving the problem of radiative transfer to determine what conditions reproduce the observed spectrum. PDR calculations typically have two free parameters: the total hydrogen density, n_H, and the strength of the UV radiation field between 6 and 13.6 eV, G_0 (where $G_0 = 1.6 \times 10^{-3}$ ergs cm^{-2} s^{-1}; Habing 1968). Once an optimal n_H and G_0 is found, the chemical and thermal structure of the PDR along with basic physical parameters such as mass, temperature, and energetics can be derived. Plane-parallel calculations like the ones presented in Kaufman et al. (1999) give contour plots showing how [O I], [C II] emission from the illuminated face (defined here as the side of the cloud facing the ionizing star or stars) along with other atomic/molecular emission-line intensities vary over a wide range of n_H and G_0. Such plots have been very useful in deriving physical conditions in a variety of galactic and extragalactic star-forming regions.

2.2. *Limits to* [O I] *and* [C II] *Diagnostic Capability*

Even with the success of PDR calculations in reproducing [O I] and [C II] observations, each line has unique features that diminish their diagnostic value. We describe the inherent problems with each line below.

[O I] 63 μm.—Liseau et al. (2006, hereafter LJT06) reviewed the results of the *Infrared Space Observatory* (*ISO*) mission and found that ~65% of the observed [O I] 63/146 emission-line ratios (hereafter $[\mathrm{O\ I}]^{63\ \mu\mathrm{m}}_{146\ \mu\mathrm{m}}$) are lower than can be explained by current models (i.e., $[\mathrm{O\ I}]^{63\ \mu\mathrm{m}}_{146\ \mu\mathrm{m}} < 10$). LJT06 found that the likely cause of this discrepancy is optical depth effects in the 63 μm line. LJT06 partially attribute the low $[\mathrm{O\ I}]^{63\ \mu\mathrm{m}}_{146\ \mu\mathrm{m}}$ observations to absorption

[1] Department of Physics, University of Cincinnati, Cincinnati, OH 45221; npabel2@gmail.com.
[2] Department of Physics, Depaul University, Chicago, IL 60614; asarma@depaul.edu.
[3] Department of Physics and Astronomy, University of Kentucky, Lexington, KY 40506; troland@pa.uky.edu, gary@pa.uky.edu.

TABLE 1
OBSERVATIONAL DATA

Parameter	Value	Reference
$\log(I_{[\mathrm{O\,I}]\,63\,\mu\mathrm{m}})$ (ergs cm^{-2} s^{-1})	-1.66 (-1.65 to -1.70)	Kraemer et al. (1998)
$\log(I_{[\mathrm{O\,I}]\,146\,\mu\mathrm{m}})$ (ergs cm^{-2} s^{-1})	-2.04 (-1.97 to -2.12)	Kraemer et al. (1998)
$\log(I_{[\mathrm{C\,II}]\,158\,\mu\mathrm{m}})$ (ergs cm^{-2} s^{-1})	-1.96 (-1.93 to -2.01)	Kraemer et al. (1998)
Q_{H} (photons s^{-1})	3×10^{48}	Rodríguez et al. (1982)
n_e(cm^{-3}) (H$^+$ region)	2×10^4	Carral et al. (2002)
Size of H$^+$ region (cm)	1.9×10^{17}	Carral et al. (2002)
A_V (mag)[a]	$445(100/T_d)$	Sandell (1999) and this work

NOTE.—A 10% correction was applied for H$^+$ region component to [C II] emission.
[a] See eq. (3).

by cold foreground O^0 in front of the 63 μm emitting region, although other explanations such as masing in the 146 μm line or very optically thick line emission cannot be ruled out. The overall conclusion from LJT06 is that because the $[\mathrm{O\,I}]^{63\,\mu\mathrm{m}}_{146\,\mu\mathrm{m}}$ line depends sensitively on detailed models, [O I] emission has a limited diagnostic value.

[O I] 146 μm.—Of the [O I] 63 and 146 μm and [C II] 158 μm emission lines, the [O I] 146 μm line is the hardest to detect in astrophysical environments. In a sample of 53 galaxies observed with *ISO*, Malhotra et al. (2001) detected the 146 μm line in only 11 galaxies. This is 4 times fewer than the number of galaxies observed in 63 μm emission. The faintness of this line diminishes its capabilities as a robust PDR diagnostic. The lower level of the 146 μm line ($J = 1$) is not the ground state of O^0, meaning that [O I] 146 μm emission is usually optically thin.

[C II] 158 μm.—The [C II] line, more than either of the [O I] lines, can be emitted by H$^+$ regions. This is particularly true in low-density gas (Heiles 1994; Abel et al. 2005; Kaufman et al. 2006; Abel 2006). This effect can hamper the use of [C II] emission as a pure PDR diagnostic in cases in which ionized and PDR gas are observed in a single spectrum. Therefore, the contribution of [C II] emission from the ionized gas must be estimated. Such an estimate requires a separate model of the H$^+$ region; although in recent years, computational methods exist that allow the H$^+$ region and PDR spectrum to be calculated self-consistently (Abel et al. 2005; Kaufman et al. 2006). Therefore, even though [C II] emission is widely observed and is usually optically thin, its dependence on the properties of the H$^+$ region can diminish its use as a PDR diagnostic.

3. NGC 6334A

The heavily obscured shell-like H$^+$ region NGC 6334A is part of a star-forming complex 1.7 kpc away. The observed [O I] and [C II] emission toward NGC 6334A ($[\mathrm{O\,I}]^{63\,\mu\mathrm{m}}_{146\,\mu\mathrm{m}} = 2.4$; see our Table 1 and Kraemer et al. 1998) cannot be explained with the geometry assumed in the widely used PDR calculations of Tielens & Hollenbach (1985a) and Kaufman et al. (1999) (see § 4.3). The close proximity and wealth of observational data for NGC 6334A make it an excellent object for enhancing our understanding of applying theoretical calculations to star-forming environments. In this section we summarize our current understanding of this region.

3.1. H$^+$ *Region*

Conditions in the H$^+$ region that are derived from radio and infrared (IR) observations are summarized in Table 1. Rodríguez et al. (1982) measured the flux at 6 cm, which they found to be consistent with an O7.5 zero-age main-sequence (ZAMS) star emitting 3×10^{48} hydrogen ionizing photons per second (Q_{H}). The size of the H$^+$ region (see next paragraph) combined with the ionizing flux yields an electron density of 2×10^4 cm^{-3}.

Previous work in the radio and submillimeter has established dimensions for the H$^+$ region and the surrounding molecular cloud. Carral et al. (2002) mapped the region in the radio continuum at 3.5 cm. They interpreted their observations as a shell with a radius of 0.06 pc (15″) and a thickness of 0.016 pc (∼2″).

3.2. *PDR and Molecular Gas*

Previous authors have observed many atomic and molecular line intensities, including [O I] (both 63 and 146 μm), [C II], and molecular transitions of CO, CS, OH, NH_3, and H_2CO. Observations of CO and CS in NGC 6334A by Kraemer et al. (1997) were interpreted as a molecular torus with dimensions of 2.2×0.9 pc. In this interpretation, the molecular torus is elongated east–west and surrounds the H$^+$ region. There are also magnetic field measurements (Sarma et al. 2000) due to the Zeeman splitting of OH at 18 cm, which absorbs bremsstrahlung emission from the background H$^+$ region at frequencies of 1665 and 1667 MHz. The [O I] and [C II] observations from Kraemer et al. (1998) are given in Table 1, with all three intensities scaled to the same beam size. Despite the breadth of observations, the physical conditions in the PDR are quite uncertain. Kraemer et al. (2000) and Sarma et al. (2000) find a total hydrogen column density $N(\mathrm{H}) = N(\mathrm{H}^0) + 2N(\mathrm{H_2}) \sim 10^{23}$ cm^{-2}, although more recent data suggests it is probable that $N(\mathrm{H_{tot}})$ exceeds 10^{24} cm^{-2} (see § 3.3) Both n_{H} and G_0 are uncertain by over an order of magnitude. The primary cause of the uncertainty is that $[\mathrm{O\,I}]^{63\,\mu\mathrm{m}}_{146\,\mu\mathrm{m}} = 2.4 \pm 0.5$. Kraemer et al. (1998) note that an adequate PDR model for NGC 6334A needs to consider the radiative transfer effects of [O I] and [C II] emission having to travel through the molecular cloud in order to reach our detectors (see § 4.1 for a discussion of geometry considerations). Kraemer et al. (2000) therefore use CO and far-IR (FIR) observations, which are less sensitive to extinction, to infer physical conditions.

3.3. A_V *toward NGC 6334A*

It is clear that A_V toward NGC 6334A is very large, with the actual value being of some debate. If we assume a dust-to-gas ratio $A_V/N(\mathrm{H_{tot}}) = 5 \times 10^{-22}$ mag cm^2 (Savage et al. 1977), then $N(\mathrm{H}) = 10^{23}$ cm^{-2} yields an $A_V \sim 50$ mag. Harvey et al. (1987) argue from near-IR observations that A_V must be at least 50 mag toward the ionizing source, while Persi et al. (2000) state that $A_V > 100$ mag.

Recent 850 μm flux maps from Sandell (1999) suggest a much higher A_V. Assuming the 850 μm emission is optically thin, the optical depth at 850 μm, τ_{850}, equals the observed intensity divided by the Planck function $B_\nu = (2h\nu^3/c^2)[\exp(h\nu/kT_d) - 1]^{-1}$, where T_d is the dust temperature. Since $h\nu/(kT_d) \ll 1$ at 850 μm,

$B_\nu \approx 2k\nu^2 T_d/c^2$. Using the observed peak flux toward NGC 6334A (15 Jy beam^{-1}, where the half-power beam width, HPBW = 14.6″), we find

$$\tau_{850} = I_{\rm obs}/B_\nu = 8 \times 10^{-3}\left(\frac{100}{T_d}\right). \quad (1)$$

We can relate τ_{850} to $N(\mathrm{H_{tot}})$ if we know how the dust extinction varies with λ. The dust opacity curve given in Figure 9 of Draine & Lee (1984) for a mixture of silicate and graphite spherical grains yields $\tau_{850} = 9 \times 10^{-27} N(\mathrm{H_{tot}})$. Equating the two expressions gives

$$N(\mathrm{H_{tot}}) = 9.0 \times 10^{23}\left(\frac{100}{T_d}\right)\ \mathrm{cm^{-2}}. \quad (2)$$

Assuming A_V and $N(\mathrm{H_{tot}})$ are related by the standard dust-to-gas ratio mentioned above, we get

$$A_V = 450\left(\frac{100}{T_d}\right)\ \mathrm{mag}, \quad (3)$$

which places useful constraints on the amount of extinction. Since dust sublimates around 10^3 K, we can place a lower limit on A_V of 45 mag. For typical $T_d = 50$–150, A_V range from 300–900 mag. This suggests that $N(\mathrm{H_{tot}})$ may be an order of magnitude higher than previously thought.

4. CALCULATIONS AND RESULTS

Our calculations use the developmental version of the spectral synthesis code Cloudy, last described by Ferland et al. (1998), to determine whether radiative transport effects of the molecular cloud on the PDR spectrum can explain the [O I] and [C II] emission-line ratios observed toward NGC 6334A. We therefore do not consider molecular emission features, such as CO or OH.

4.1. *Abundances and Stopping Criteria*

Our assumed gas-phase abundances are an average from the work of Cowie & Songalia (1986) and Savage & Sembach (1996). The two most important abundances for this calculation, oxygen and carbon, have assumed gas-phase abundances (relative to hydrogen) of 3.2×10^{-4} and 2.5×10^{-4}, respectively. We assume a galactic ratio of visual extinction to hydrogen column density, $A_V/N(\mathrm{H_{tot}})$, of 5×10^{-22} mag cm^2. Grain-size distributions for gas adjacent to H$^+$ regions, such as Orion (Cardelli et al. 1989) tend to have a larger ratio of total to selective extinction than observed in the ISM. We therefore use a truncated MRN grain size distribution (Mathis et al. 1977) with $R = 5.5$, which reproduces the Orion extinction curve (Baldwin et al. 1991). We also include size-resolved polycyclic aromatic hydrocarbons (PAHs) in our calculations, with the same size distribution used by Bakes & Tielens (1994). The abundance of carbon atoms in PAHs that we use, $n_{\rm C}(\mathrm{PAH})/n_{\rm H}$, is 3×10^{-6}. PAHs are thought to be destroyed by hydrogen ionizing radiation and coagulate in molecular environments (see, e.g., Omont 1986). We model this effect by scaling the PAH abundance by the ratio of $\mathrm{H^0/H_{tot}}$ ($n_{\rm C}(\mathrm{PAH})/n_{\rm H} = 3 \times 10^{-6}[n(\mathrm{H^0})/n(\mathrm{H_{tot}})]$).

We predict the PDR emission-line spectrum for increasing hydrogen column densities, which we give in terms of A_V (by assuming the gas-to-dust ratio given in § 3.3). We initially stop the model when $A_V = 1$ mag, and then increase A_V by a factor of 1.5 until we reach $A_V \sim 1500$ mag. This allows us to consider the range of possible extinctions given by equation (3). Our calculations include a turbulent line width $v_{\rm turb} = 3$ km s^{-1}, which is consistent with the observed OH absorption line width toward NGC 6334A observed by Sarma et al. (2000). The effect of $v_{\rm turb}$ is to reduce the predicted line optical depth, since τ and line width are inversely proportional.

4.2. *Radiation Field and Density*

The shape and intensity of the UV continuum for NGC 6334A is highly uncertain (see references in §§ 3.1 and 3.2). Because of the uncertainty in the incident continuum and because we are primarily interested in the transport of the PDR lines through the molecular cloud and not the exact nature of the continuum shape, we chose the widely used Draine (1978) ultraviolet (UV) radiation field in our calculations. The Draine continuum contains no hydrogen ionizing radiation and is defined over the energy range 5–13.6 eV. The relationship between the Draine field (hereafter χ) and G_0 is $G_0 = 1.71\chi$ (Bertoldi & Draine 1996). We consider two values for G_0: $10^{4.5}$ and $10^{5.5}$. These values are consistent with the range of G_0 given in Kraemer et al. (2000) of $10^{4.0}$–$10^{6.2}$, based on the estimated G_0 from an O7.5 star and the PDR models of Kaufman et al. (1999).

To account for hot dust emission from the H$^+$ region, we include a $T = 75$ K blackbody with a total intensity of 5×10^2 ergs cm^{-2} s^{-1}. This is identical to the dust continuum used by Tielens & Hollenbach (1985b), used to model the dust emission coming from the Orion H$^+$ region. We found that, although the dust continuum increased the total luminosity of the system, it made little or no difference in the predicted [O I] and [C II] emission-line intensities. The only other ionization source considered is cosmic rays. We include primary and secondary cosmic-ray ionizations as described in Appendix C of Abel et al. (2005), with a cosmic-ray ionization rate of 5×10^{-17} s^{-1}.

Since our calculations do not consider hydrogen-ionizing radiation, we had to estimate the portion of [C II] emission which is due to the ionized gas. The high n_e of the shell H$^+$ region, combined with the measured $Q(\mathrm{H})$ and radius, suggests most of the [O I] and [C II] emission comes from the PDR and not the H$^+$ region (Abel et al. 2005; Kaufman et al. 2006; Abel 2006; see also Table 1). We use the results of Abel (2006), which calculate the percentage of [C II] emission from H$^+$ regions as a function of H$^+$ density, ionization parameter U ($U = Q_{\rm H}/[4\pi r^2 n_e c]$), stellar temperature T^*, and stellar atmosphere. With the values of $Q_{\rm H}$, r, and n_e given in Table 1, we find $U \approx 10^{-1.9}$. In addition, the observed $Q_{\rm H}$ corresponds approximately to $T^* = 35,000$ K (Vacca et al. 1996). Using these values and Figure 2 of Abel (2006), we find 5%–15% of the total [C II] emission comes from the H$^+$ region. We therefore adopt the value of 90% for observed [C II] emission that comes from the PDR.

The remaining free parameter in our calculations is $n_{\rm H}$. Our primary interest is to determine if a single-component model for NGC 6334A can explain the observed [O I] and [C II] emission. We therefore assume that $n_{\rm H}$ is constant throughout our calculations and consider values of $10^{4.0}$, $10^{5.0}$, and $10^{6.0}$ cm^{-3}. Such a density profile is an approximation to regions where magnetic or turbulent pressure dominates (Tielens & Hollenbach 1985a). A real molecular cloud is not homogeneous, but rather a clumpy, dynamically evolving entity. Our choice of $n_{\rm H}$, therefore, represents an average over the physical extent of the cloud. We explore the effects of a density power law on the best-fitting single-component calculation in § 5.2. Overall, our choice of $n_{\rm H}$, G_0, and stopping A_V represents a total of 114 different calculations.

The most detailed calculation for NGC 6334A would also include the ionized gas and connect the H$^+$ region to the PDR through an equation of state such as constant pressure (Abel et al. 2005;

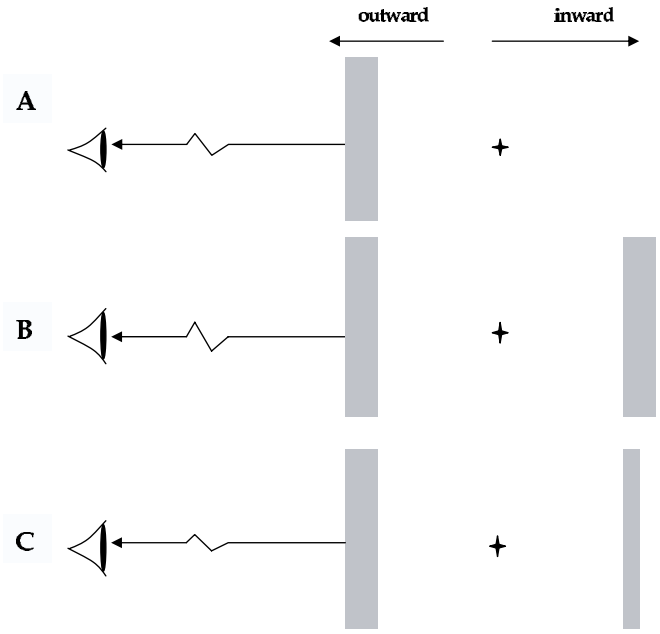

FIG. 1.—Three possible geometries for NGC 6334A considered in this paper. These scenarios are an open geometry, in which radiation freely escaped out the hot, illuminated face (inward direction) but is optically thick in the outward direction (*a*), a closed geometry, in which the radiation is smothered on both sides by a thick molecular cloud (*b*), or an asymmetric geometry, in which the molecular cloud is not as thick on one side (*c*). Our calculations presented in § 5 assume the geometry from (*b*).

Kaufman et al. 2006). There are two reasons we chose to ignore the H^+ region in this work. For one, we wanted to compare our results to other PDR calculations, in particular Tielens & Hollenbach (1985a), Kaufman et al. (1999), and LJT06, all of which do not include the H^+ region. Secondly, we wanted to demonstrate an application of Abel et al. (2005) and Abel (2006) in estimating the percent emission of [C II] from the H^+ region if both U and n_e are known. The proximity and amount of observational data for NGC 6334A makes the region an excellent case study.

4.3. *Geometry Considerations*

The usual geometry assumed in PDR calculations is a single-sided plane-parallel slab (see Tielens & Hollenbach 1985a; geometry shown in Fig. 1*a*). We refer to this geometry as an "open geometry." An open geometry is a good approximation to "blister H^+ regions" adjacent to PDRs (Tielens & Hollenbach 1985b) such as Orion. For an open geometry, it is convenient to define the direction toward the star as "inward" and the direction away from the star as "outward" (see Fig. 1*a*). Using this nomenclature, the [O I] 63 μm emission is very optically thick in the outward direction, forcing all the [O I] emission to become beamed in the inward direction. The [O I] 145 μm and [C II] 158 μm lines have smaller optical depths, therefore allowing a small fraction of photons to escape in the outward direction. The predicted line intensity is presented as the emergent flux in the inward direction, divided by 2π (Kaufman et al. 1999).

The other possible geometry is one in which the PDR emitting region is completely surrounded by a large column density of molecular gas. We refer to this geometry as a "closed geometry." A similar geometry is used in Doty & Neufeld (1997) in the modeling of dense molecular cores. In a closed geometry, all energy eventually escapes in the direction outward from the star.

For both the open and closed geometries, we assume the velocity field of the PDR is the same as the molecular cloud. We refer to this assumption as a "static geometry." Assuming a static geometry is justified, since the observed line widths for H I and OH absorption, along with H_2CO emission, are nearly identical (de Pree et al. 1995; Sarma et al. 2000). This indicates the broadening of both regions is dominated by turbulence.

It is improbable that the PDR emitting region is exactly at the center of the molecular cloud. Instead, the true geometry is likely to be asymmetric, with the ionizing stars being closer to one side of the molecular cloud (Fig. 1*c*). Observations suggest that the H^+ region is located closer to the back side than to the front side of the molecular cloud. In particular, the radio-frequency recombination-line observations of de Pree et al. (1995) show that the southern lobe of ionized gas is redshifted relative to the central H^+ region by about 10 km s^{-1}. Such a redshift is most naturally explained if the H^+ region is located near the back side of the cloud and has opened a hole in the cloud through which ionized gas is expanding away from the observer. We discuss the implications of an asymmetric geometry where the thicker part of the molecular cloud is along our line of sight in § 5.2.

4.4. *Open-Geometry Results*

It is possible that NGC 6334A is simply an open geometry, such as a blister H^+ region, where we observe the H^+ region through the molecular cloud. Such a scenario would be akin to observing Orion rotated 180°, from the perspective of being on the opposite side of OMC 1. If true, then this geometry must lead to an outward $[\mathrm{O\ I}]^{63\ \mu\mathrm{m}}_{146\ \mu\mathrm{m}} = 2$–3 for physically plausible values of A_V, as defined by equation (3).

We performed an open-geometry PDR calculation to determine if the outward $[\mathrm{O\ I}]^{63\ \mu\mathrm{m}}_{146\ \mu\mathrm{m}}$ ratio could be due to emission from a blister H^+ region on the far side of NGC 6334A. The parameters for the model were $n_{\mathrm{H}} = 10^5$ cm^{-3} and $G_0 = 10^5$, with abundances and other physical parameters treated as described in §§ 4.1 and 4.2.

Figure 2 shows the predicted [O I] intensities in the inward and outward directions, along with the total emission. Figure 2 shows just how sensitive the 63 μm line is to optical depth effects. For extremely low values of A_V, some 63 μm emission escapes through the outward direction. For $A_V > 5$, however, the [O I] line becomes optically thick, and over 90% of the 63 μm emission is beamed in the inward direction. The [O I] 145 μm remains essentially optically thin throughout, with the inward emission only slightly greater than the outward component.

The combined radiative transfer effects of the two [O I] lines are shown by Figure 3, which plots $[\mathrm{O\ I}]^{63\ \mu\mathrm{m}}_{146\ \mu\mathrm{m}}$ for the inward direction, outward direction, and total. The inward direction, corresponding to the geometry assumed in most PDR calculations, predicts a constant $[\mathrm{O\ I}]^{63\ \mu\mathrm{m}}_{146\ \mu\mathrm{m}}$. The predicted inward $[\mathrm{O\ I}]^{63\ \mu\mathrm{m}}_{146\ \mu\mathrm{m}}$ also exceeds the optically thin limit of 10. The outward $[\mathrm{O\ I}]^{63\ \mu\mathrm{m}}_{146\ \mu\mathrm{m}}$ ratio, which is what would be observed toward NGC 6334A, is orders of magnitude lower and depends sensitively on A_V.

Figure 3 essentially rules out an open geometry. If NGC 6334A were a blister H^+ region observed through the molecular cloud, then the observed $[\mathrm{O\ I}]^{63\ \mu\mathrm{m}}_{146\ \mu\mathrm{m}}$ ratio would imply an A_V of 10–20 mag, which is incompatible with the observed 850 μm emission (eq. [3]), as it would yield $T_d = (2\text{–}4) \times 10^3$ K, which exceeds the dust sublimation temperature. This ratio should depend primarily on the amount of extinction and only weakly on n_{H} or G_0. The extinction will depend somewhat on line width (v) and the O/H abundance ratio. A turbulent line width of 3 km s^{-1} was used in the calculation and is based on observations (§ 4.2). Therefore, the only free parameter that could alter this conclusion is the O/H ratio, which would have to be $\sim 10^{-6}$ in order to permit a high

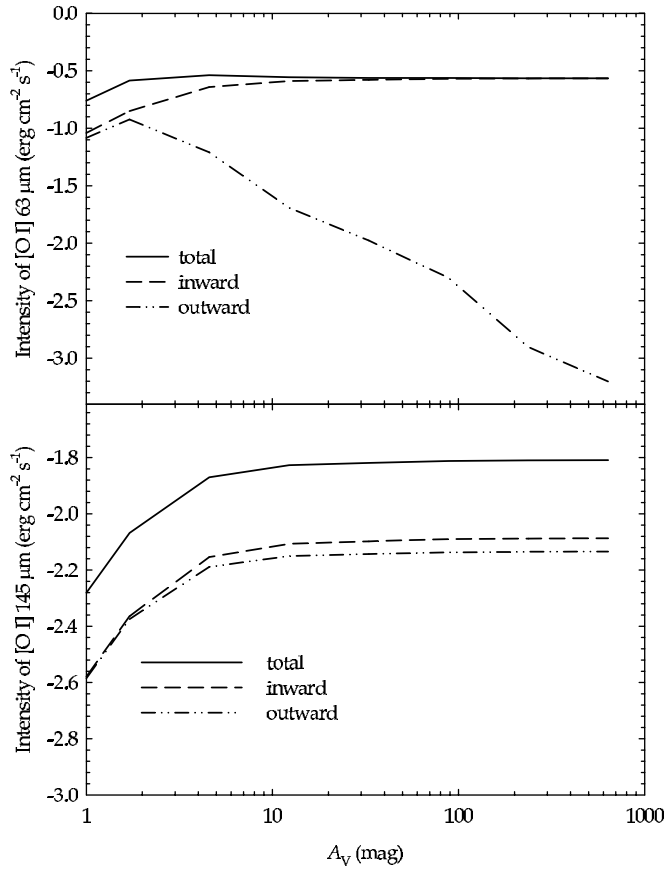

FIG. 2.—Intensity of [O I] lines as a function of A_V, for the open geometry shown in Fig. 1*a*. The outward component of the 63 μm line falls off rapidly with A_V, due to the large optical depth in the outward direction, which beams all 63 μm emission in the inward direction. The 145 μm line has a much smaller optical depth in the outward direction, meaning it can escape freely in either direction. This is shown by the inward and outward intensities being approximately equal.

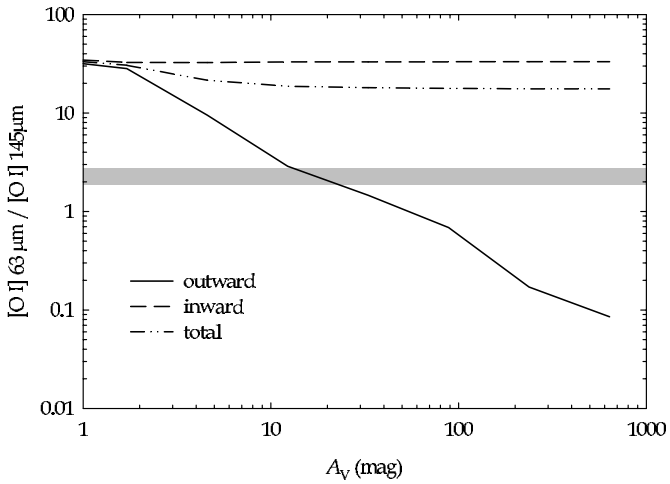

FIG. 3.—The $[\mathrm{O\ I}]^{63\,\mu\mathrm{m}}_{146\,\mu\mathrm{m}}$ ratio in the inward and outward directions, along with the total, for the open geometry shown in Fig. 1*a*. The inward direction shows the ratio in the optically thin inward direction remaining >10, which is what is usually reported in plane-parallel PDR calculations. Since all 63 μm emission is beamed in the outward direction (Fig. 2), $[\mathrm{O\ I}]^{63\,\mu\mathrm{m}}_{146\,\mu\mathrm{m}}$ decreases dramatically with A_V. The horizontal gray bar represents the observed $[\mathrm{O\ I}]^{63\,\mu\mathrm{m}}_{146\,\mu\mathrm{m}}$ ratio toward NGC 6334A. This shows that for $A_V > 30$ mag, the predicted ratio falls below the observed limits. This low A_V is incompatible with 850 μm observations (eq. [3]).

TABLE 2
BEST-FIT CONSTANT-DENSITY MODEL

Parameter	Value
$\log(I_{[\mathrm{O\ I}]\ 63\ \mu\mathrm{m}})$	−1.67
$\log(I_{[\mathrm{O\ I}]\ 146\ \mu\mathrm{m}})$	−2.02
$\log(I_{[\mathrm{C\ II}]\ 158\ \mu\mathrm{m}})$	−1.95
n_{H}	$10^{5.7}$
G_0 ($1G_0 = 1.71\chi$)	7×10^4
$N(\mathrm{H})$	1.3×10^{24} (cm^{-2})
Physical thickness (L)	0.8 pc
A_V	650 mag

enough A_V to be consistent with the 850 μm emission. Such an O/H ratio is unphysically low.

4.5. *Closed-Geometry Results*

The results of our closed-geometry calculations are shown in Figures 4–7 and Table 2. Table 2 gives the set of parameters (n_{H}, G_0, and A_V) that best fits the observed spectrum, along with the predicted [O I] and [C II] emission-line intensities.

Figures 4–6 show the predicted [O I] and [C II] emission-line intensities as functions of n_{H}, G_0, and A_V. Increasing either n_{H} or G_0 increases the line intensity, which is typical for PDR calculations (Tielens & Hollenbach 1985a; Kaufman et al. 1999). As the density is decreased, the size of the [O I] emitting region increases,

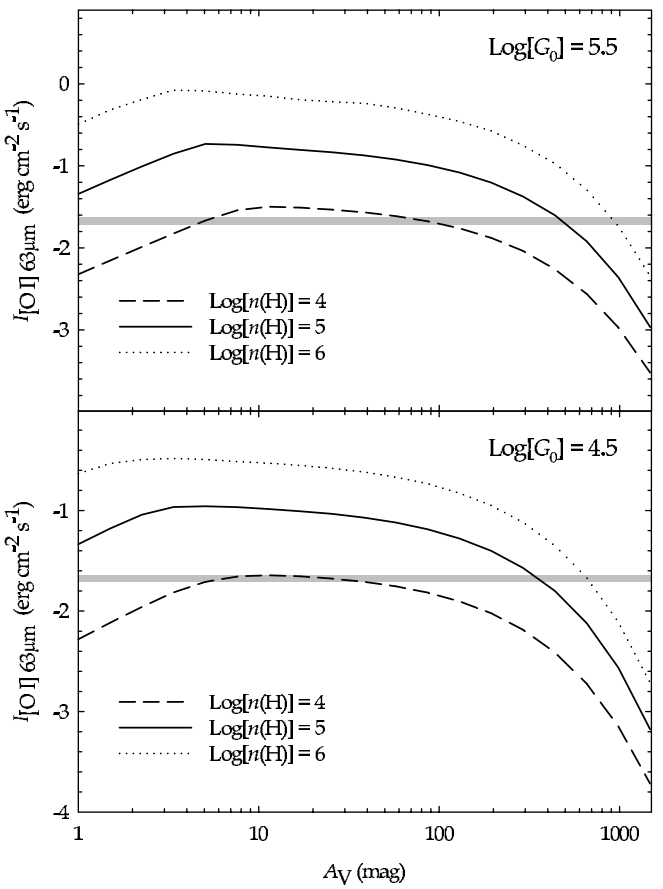

FIG. 4.—Emergent intensity of [O I] 63 μm line for $n_{\mathrm{H}} = 10^{4.0}$, $10^{5.0}$, and $10^{6.0}$ cm^{-3} and $G_0 = 10^{4.5}$ and $10^{5.5}$ as a function of A_V. The horizontal gray bar represents the observed 2 σ range. The intensity increases with increasing n_{H} or G_0, as expected. For larger A_V, the increased line optical depth reduces the observed intensity. For $A_V = 1477$ mag, the 63 μm optical depth is ≈250.

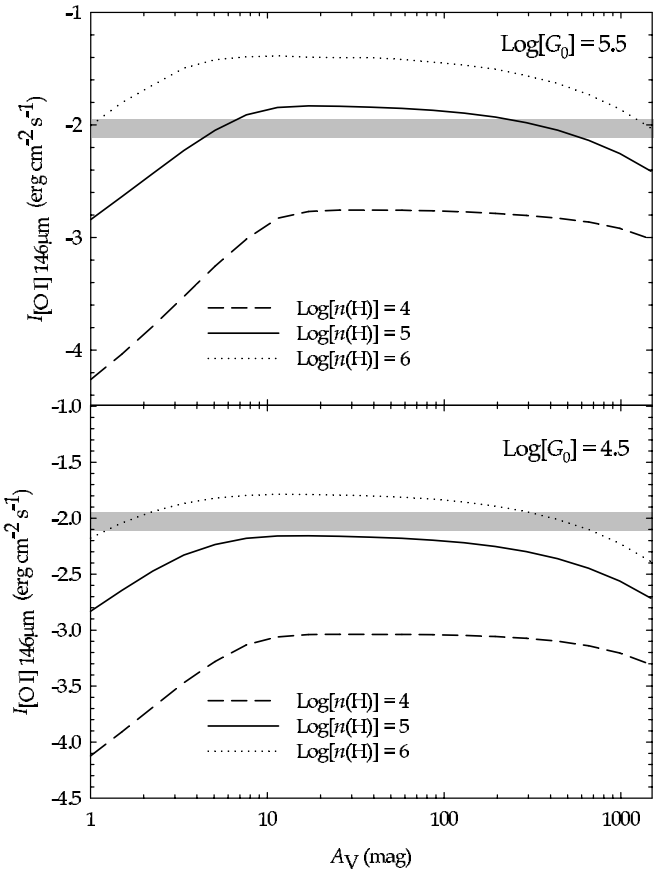

FIG. 5.—Emergent intensity of the [O I] 146 μm line for $n_H = 10^{4.0}$, $10^{5.0}$, and $10^{6.0}$ cm^{-3} and $G_0 = 10^{4.5}$ and $10^{5.5}$ as a function of A_V. The horizontal gray bar represents the observed 2 σ range. The intensity increases with increasing n_H or G_0, as expected. For larger A_V, the increased line optical depth reduces the observed intensity; however, line optical depth effects are much less important for this line than for 63 μm emission. For $A_V = 1477$ mag, the 146 μm optical depth is $\approx$2.5.

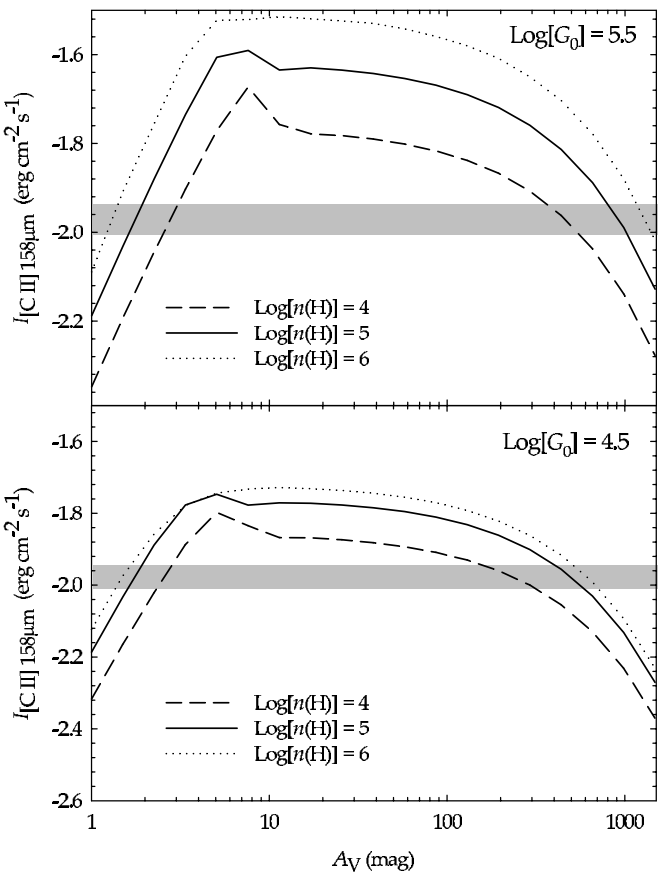

FIG. 6.—Intensity of [C II] 158 μm line for $n_H = 10^{4.0}$, $10^{5.0}$, and $10^{6.0}$ cm^{-3} and $G_0 = 10^{4.5}$ and $10^{5.5}$ as a function of A_V. The horizontal gray bar represents the observed 2 σ range. The intensity increases with increasing n_H or G_0, as expected. For larger A_V, the increased line optical depth reduces the observed intensity. This effect is much less than for 63 μm emission, since most carbon is not in the form of C^+, but rather C^0 and CO. For $A_V = 1477$ mag, the 158 μm optical depth is $\approx$1.6.

because the size of the H^0 region, which is where [O I] and [C II] emission forms, is proportional to the ratio G_0/n_H. Lowering n_H results in less H_2 shielding, producing a larger H^0 region and shifting the peak emission to larger depths (typically $A_V = 2$–10, with 10 corresponding to log $[n_H] = 4$). For larger A_V, line optical depths reduce the emergent intensity. As expected, line optical depth effects are largest for the [O I] 63 μm emission line (Fig. 2). Our calculations show the 63 μm intensity decreases by over 2 orders of magnitude, with $\tau_{63\ \mu m} = 250$ for $A_V = 1500$ mag. The large optical depth is due to the large O^0 ($J = 2$) column density and not due to either self-absorption or absorption by dust.

This decrease in emergent intensity of the [O I] 63 μm line is due to the large optical depth of the line as the O^0 column density increases. Increasing τ reduces the critical density (n_{crit}) of the 63 μm line by τ (Osterbrock & Ferland 2006). For the 63 μm line, $n_{crit} = 5 \times 10^5$ cm^{-3}, which means that for the range of densities considered, $n_H > n_{crit}$ for large A_V. We refer to this effect as the line becoming "thermalized," as the large optical depth leads to the $^3P_1$ state, preferentially deexciting through collisions instead of through photon emission. In addition to thermalization of the 63 μm line, there is also the fact that for large τ the line will emit like a blackbody at the local temperature (typically a few tens of kelvin). We can only see the 63 μm line emerging from regions of a few optical depths. Therefore, for increasing A_V, the temperature decreases and the emergent intensity of the 63 μm line is reduced.

Line optical depths are less important for the [O I] 146 μm and [C II], although both lines do eventually become optically thick. At $A_V = 1500$ mag, $\tau \sim 2.5$ for [O I] 146 μm and $\tau \sim 1.6$ for [C II]. The reason for the lower optical depth is that there are much fewer O^0 atoms in the $J = 1$ state of O^0 capable of increasing the 146 μm optical depth. Extinction effects for [C II] are similar to [O I] 146 μm, with one important difference. Carbon is primarily in the form of C^+ in H^0 regions, with C^+ converted into C^0 and CO beyond the H^0/H_2 molecular front. This leads to optical depth effects reducing 158 μm emission in this region, which manifests itself as a decrease in the emergent intensity just beyond the peak. Once C^+ is converted to C^0 and CO, the effects of extinction are reduced and only become significant when A_V is large.

Figure 7 shows how $[\mathrm{O\ I}]^{63\ \mu m}_{146\ \mu m}$ ratio varies with increasing A_V. The dependence of $[\mathrm{O\ I}]^{63\ \mu m}_{146\ \mu m}$ on G_0 is weak, which is expected for the range of n_H and G_0 we consider (see Fig. 5 of Kaufman et al. 1999). For low A_V, $[\mathrm{O\ I}]^{63\ \mu m}_{146\ \mu m}$ is a factor of 3 higher for the log $[n_H] = 4$ case than for densities of log $[n_H] = 5$ or 6, because for log $[n_H] = 4$, the [O I] line emitting region extends out to $A_V \sim 10$. Therefore, to compare our calculations to Kaufman et al. (1999), we need to compare the predicted $[\mathrm{O\ I}]^{63\ \mu m}_{146\ \mu m}$ ratio at the depth where both lines have fully formed but have not yet suffered from extinction effects. This depth corresponds to the peak [O I] emission shown in Figures 4 and 5. As mentioned above, the peak [O I] emission for log $[n_H] = 4$ is $A_V \sim 10$, while for log $[n_H] = 5$ or 6 the peak is located around $A_V \sim 2$–4. Using

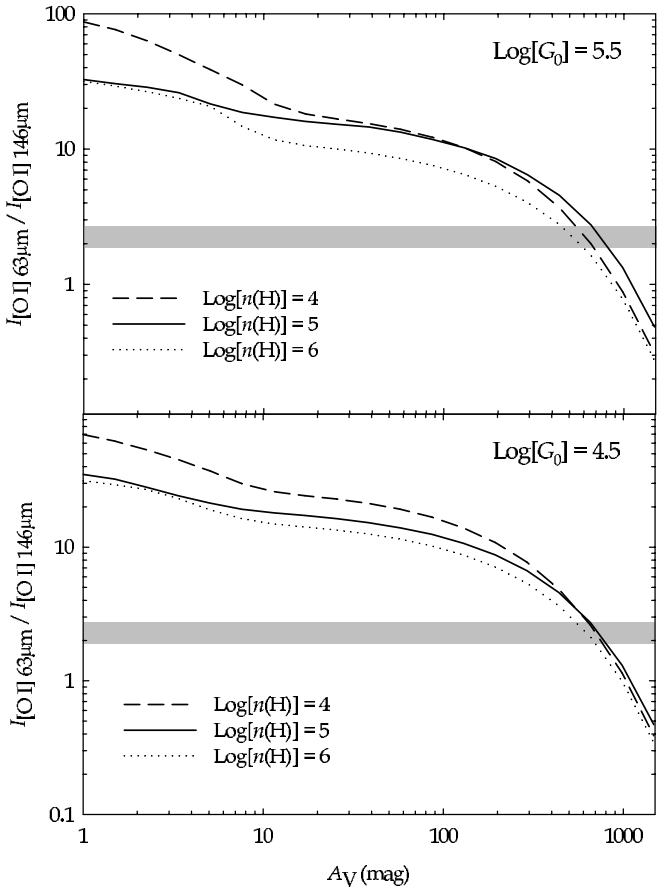

FIG. 7.—Ratio of $[\mathrm{O\ I}]^{63\ \mu\mathrm{m}}_{146\ \mu\mathrm{m}}$ for $n_{\mathrm{H}} = 10^{4.0}$, $10^{5.0}$, and $10^{6.0}$ cm^{-3} and $G_0 = 10^{4.7}$ and $10^{5.7}$ as a function of A_V. The horizontal gray bar represents the observed 2 σ range. To a good approximation, $[\mathrm{O\ I}]^{63\ \mu\mathrm{m}}_{146\ \mu\mathrm{m}}$ is independent of G_0 for the range of n_{H} and G_0 considered. As the amount of extinction increases, the O^0 column density increases. This leads to a larger [O I] 63 μm optical depth and a reduction in $[\mathrm{O\ I}]^{63\ \mu\mathrm{m}}_{146\ \mu\mathrm{m}}$.

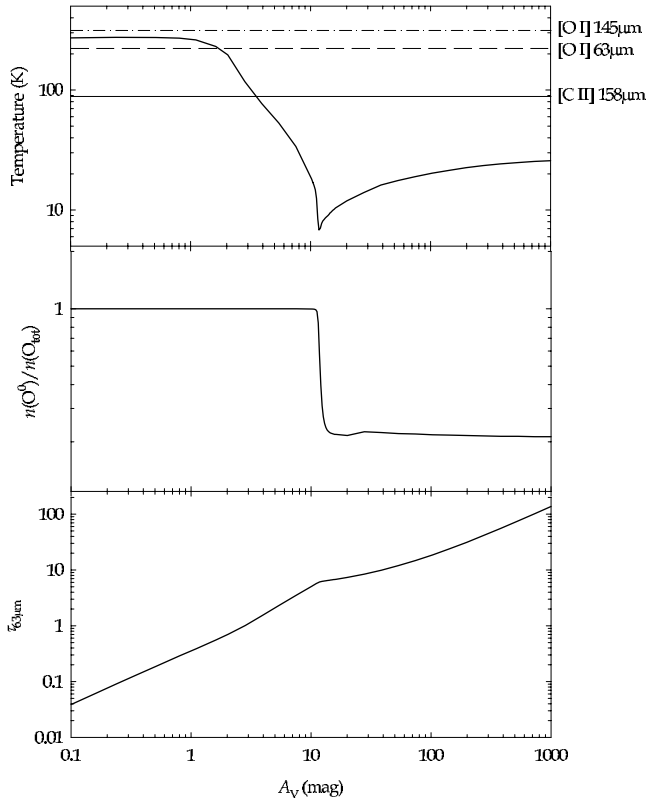

FIG. 8.—Temperature, O^0 fraction, and [O I] 63 μm optical depth as a function of A_V for the best-fit model for a constant-density, closed-geometry model given by Table 2. The horizontal lines on the temperature plot represent the temperature required to reach the upper level of the [C II] 158 μm and [O I] 63 and 146 μm transition.

Figure 7, we find $[\mathrm{O\ I}]^{63\ \mu\mathrm{m}}_{146\ \mu\mathrm{m}}$ is nearly constant for the depth where [O I] emission peaks. This also agrees fairly well with Figure 5 of Kaufman et al. (1999). Beyond the peak, the increased optical depth for [O I] 63 μm (see Fig. 4) causes $[\mathrm{O\ I}]^{63\ \mu\mathrm{m}}_{146\ \mu\mathrm{m}}$ to fall below the optically thin limit of 10 (LJT06).

Our calculations allow us to find a set of physical parameters that reproduce the observed 1 σ [O I] and [C II] emission-line spectrum (Figs. 4–7, *horizontal gray bars*). Looking at Figure 7, we can see that we need A_V to be between 400 and 800 mag in order to reproduce the observed $[\mathrm{O\ I}]^{63\ \mu\mathrm{m}}_{146\ \mu\mathrm{m}}$. Figures 4 and 5 eliminate $n_{\mathrm{H}} = 10^{4.0}$ cm^{-3}, since the predicted intensity is too low given the requirement for A_V. Figures 4–7 show that the model with $G_0 = 10^{4.5}$, $n_{\mathrm{H}} = 10^{6.0}$ cm^{-3}, and $A_V \sim 600$–700 mag approximately reproduces the [O I] and [C II] emission. Using these values as a guide, we varied n_{H}, G_0, and A_V around these values to find a set of n_{H}, G_0 that reproduces the observed intensities to within 2 σ, with our derived quantities. The best values are $n_{\mathrm{H}} = 10^{5.7}$ cm^{-3}, $G_0 = 10^{4.8}$, and $A_V = 650$ mag and are given in Table 2.

Figure 8 shows the gas temperature, [O I] 63 μm optical depth, and the fraction of O and C in the form of O^0 and C^+ for the best-fit parameters given in Table 2. The temperature decreases with increasing A_V, falling well below the excitation temperature for the two [O I] emission lines for $A_V > 2$–5, meaning nearly all the emission occurs for $A_V < 5$ mag. The fractional abundance of O in atomic form remains significant throughout the cloud complex, although the formation of CO reduces the O^0 abundance to 20% of its initial value. We included condensation of molecules onto grain surfaces (see Abel et al. [2005] for a description of how this is incorporated into Cloudy) in our modeling, which made no difference in the O^0 abundance with depth. The combination of low temperature and high O^0 abundance leads to a significant ground state O^0 column density, which in turn yields a large [O I] 63 μm optical depth. The increase in optical depth with A_V is not linear, because the formation of CO, which decreases the O^0 abundance and, therefore, the ratio of [O I] 63 μm optical depth per A_V.

We can compare our derived values of n_{H} and A_V with LJT06 calculations of optically thick [O I] emission. Figure 4 of LJT06 shows $[\mathrm{O\ I}]^{63\ \mu\mathrm{m}}_{146\ \mu\mathrm{m}}$ as a function of temperature in the case in which both [O I] lines are either optically thick or optically thin. The calculations presented in this work show the transition from optically thin emission, to optically thick [O I] 63 μm emission but optically thin [O I] 146 μm emission, and finally to the regime in which both lines are optically thick. Figure 5 shows the value of $N(\mathrm{H}^0)$ necessary to get an [O I] 146 μm optical depth of unity. LJT06 predicts the NGC 6334A observed $[\mathrm{O\ I}]^{63\ \mu\mathrm{m}}_{146\ \mu\mathrm{m}}$ ratio for a temperature of $\sim$50 K. At this temperature, LJT06 predicts optically thick [O I] 146 μm for $N(\mathrm{H}^0) \sim 10^{24}$ cm^{-2} and $n_{\mathrm{H}} = 10^{5.5}$–$10^{6.0}$. Our results therefore appear to agree with the calculations shown in LJT06.

Our results show that the observed [O I] and [C II] spectrum can be explained by a constant-density PDR calculation combined with a closed geometry in which the PDR emission must travel through a large column density of molecular gas. The derived $A_V = 650$ mag corresponds to a dust temperature of 70 K. This A_V also corresponds to $N(\mathrm{H_{tot}}) = 10^{24.1}$ cm^{-2}, which corresponds to a physical thickness $L = N(\mathrm{H_{tot}})/n_{\mathrm{H}}$ of $\sim$0.8 pc, within

TABLE 3
DEPENDENCE OF NGC 6334A MODEL ON DENSITY LAW

PARAMETER	VALUE FOR $\alpha =$				
	-2	-1.5	-1	-0.5	0
r_c (pc)[a]	0.95	0.65	0.30	0.10	...
$\log(I_{[\mathrm{O\ I}]\ 63\ \mu\mathrm{m}})$	-1.56	-1.56	-1.56	-1.56	-1.67
$\log(I_{[\mathrm{O\ I}]\ 146\ \mu\mathrm{m}})$	-1.96	-1.96	-1.96	-1.96	-2.02
$\log(I_{[\mathrm{C\ II}]\ 158\ \mu\mathrm{m}})$	-1.93	-1.93	-1.93	-1.93	-1.95

[a] Density law given by eq. (4).

20%–30% of the size of the molecular torus in the plane of the sky (1.1 pc; see Fig. 1). Overall, the density, radiation field, column density, and physical thickness are consistent with previous studies of the region.

5. SENSITIVITY TO MODEL ASSUMPTIONS

5.1. *Effects of Density Law*

While a single-component PDR model can explain the observed [O I] and [C II] emission, it is highly unlikely that the density is uniform throughout the entire molecular complex. At the very least, the line of sight toward NGC 6334A is clumpy (Kraemer et al. 1997). Both observational and theoretical evidence suggest the density in molecular clouds follows some power-law dependence on density ($n \propto r^{\alpha}$; see Doty & Neufeld 1997 and references therein), with $\alpha \sim -2$. In the study of 14 envelopes around massive stars, van der Tak et al. (2000) found $\alpha \sim -1.0$, -1.5 best fit the observations. A density gradient will change the predicted chemical/thermal structure of the cloud, which will have consequences for the predicted [O I] and [C II] emission.

We explored the effects of a density law on the best-fitting, constant-density model. We chose a density law of the form

$$n(\mathrm{H})_r = n(\mathrm{H})_0 \left(1 + \frac{r}{r_c}\right)^{\alpha} \ \mathrm{cm}^{-3}, \qquad (4)$$

where r is the depth into the cloud, r_c is the thickness over which the density remains relatively constant, and $n(\mathrm{H})_0$ and $n(\mathrm{H})_r$ are the hydrogen densities at the illuminated face and at a given depth, respectively. Density laws of this form are commonly assumed in the study of hot molecular cores (see Nomura & Millar 2004 and references therein).

We constrained our density-law parameters in order to make a direct comparison between the best-fitting constant-density models. We considered four values for α: -2, -1.5, -1, and -0.5. We required that each calculation reproduce $N(\mathrm{H})$ (and hence A_V) given by the best single-component model. We also required that the model stop at the thickness given by the single-component model, which allows us to compare calculations with the same average density as the single-component model. We chose $n(\mathrm{H})_0 = 10^6$ cm^{-3}, which would be the PDR surface density if the H$^+$ region and PDR were in gas-pressure equilibrium with $T(\mathrm{H}^+) = 10^4$ K and $T(\mathrm{PDR}) = 200$ K. There is a unique value of r_c (for each α) which satisfies our constraints, and these values are given in Table 3.

The results of our density-law calculations are given in Table 3. We find that a density law increases the predicted PDR line intensities, with a 0.11 dex increase in $I_{[\mathrm{O\ I}]\ 63\ \mu\mathrm{m}}$, a 0.06 dex increase in $I_{[\mathrm{O\ I}]\ 145\ \mu\mathrm{m}}$, and a 0.02 dex increase in $I_{[\mathrm{C\ II}]\ 158\ \mu\mathrm{m}}$. However, we also find, for $\alpha \neq 0$, that the predicted intensities are independent of α. This is due to the fact that for all α the [O I] and [C II] emission emerges from a region with the same value of n_{H} (10^6 cm^{-3}) and G_0 ($10^{5.2}$). In addition, since we kept the total column density fixed, the effects of extinction were nearly identical for each model. If we had chosen the density from the constant-density model as $n(\mathrm{H})_0$ and stopped at $A_V = 650$ mag, we would have reproduced the observed PDR spectrum. However, the physical thickness required to reproduce an A_V this high is much larger than the constant-density model (10 pc for $\alpha = -2$ and 3 pc for $\alpha = -0.5$; compared to 0.8 pc for the constant-density model). Such a model would also yield a lower average $n(\mathrm{H})$, $\overline{n(\mathrm{H})}$, although the average would still exceed 10^5 cm^{-3}.

TABLE 4
DEPENDENCE OF $\alpha = -2$ NGC 6334A MODEL ON EXTINCTION

A_V (mag)	$\log(I_{[\mathrm{O\ I}]\ 63\ \mu\mathrm{m}})$	$\log(I_{[\mathrm{O\ I}]\ 146\ \mu\mathrm{m}})$	$\log(I_{[\mathrm{C\ II}]\ 158\ \mu\mathrm{m}})$
550	-1.41	-1.92	-1.90
600	-1.49	-1.94	-1.92
650	-1.56	-1.96	-1.93
700	-1.63	-1.98	-1.95
750	-1.70	-1.99	-1.97

We performed a final test to see if a density-law model could reproduce the observed PDR emission-line spectrum. We took the $\alpha = -2$ power law with $n(\mathrm{H})_0 = 10^6$ cm^{-3} and allowed A_V to increase beyond the single-component model $A_V = 650$ mag. Table 4 summarizes our results. Increasing A_V increases the line optical depths, thereby reducing the emergent intensity. For $A_V = 700$–750, the density-law and constant-density model predict nearly identical [O I] and [C II] line intensities, which in turn agree with observations. Therefore, we conclude that the effects of a density law are to increase A_V [or $N(\mathrm{H})$].

5.2. *Effects of an Asymmetric Geometry*

The closed and open geometry are the two limiting geometries, while an asymmetric geometry (Fig. 1*c*) is the intermediate case. Section 4.4 showed that in a pure open geometry an A_V of 20 between us and the ionizing stars reproduces the observed $[\mathrm{O\ I}]^{63\ \mu\mathrm{m}}_{146\ \mu\mathrm{m}}$, while $A_V = 650$ reproduces the observed $[\mathrm{O\ I}]^{63\ \mu\mathrm{m}}_{146\ \mu\mathrm{m}}$ for a closed geometry. As argued in § 4.3, the asymmetric case is one in which more molecular material lies between us and the ionizing stars (near side) than between the ionizing stars and the back of the molecular cloud (back side). The asymmetric case differs from the open geometry in that the back side of the cloud no longer has radiation freely escaping. Instead, the back side can also become optically thick to [O I] 63 μm emission. This leads to more [O I] emission escaping out the near side, increasing the observed $[\mathrm{O\ I}]^{63\ \mu\mathrm{m}}_{146\ \mu\mathrm{m}}$. Therefore, the amount of A_V needed to reproduce the observed $[\mathrm{O\ I}]^{63\ \mu\mathrm{m}}_{146\ \mu\mathrm{m}}$ for the asymmetric geometry is greater than the pure open case ($A_V > 20$). The asymmetric geometry also differs from the closed geometry in an important way. In a closed geometry, the [O I] 63 μm optical depth toward the near or back side is the same. In the asymmetrical case, the optical depth in the back side of the cloud is less than in the near side. This leads to more [O I] 63 μm emission escaping out the back side than the near side, which lowers $[\mathrm{O\ I}]^{63\ \mu\mathrm{m}}_{146\ \mu\mathrm{m}}$. Therefore, the amount of A_V needed to reproduce the observed $[\mathrm{O\ I}]^{63\ \mu\mathrm{m}}_{146\ \mu\mathrm{m}}$ for the asymmetric geometry is less than the pure closed case ($A_V < 650$).

Overall, our results place several constraints on A_V. Based on geometrical considerations, A_V can range from 20 to 650, with 650

being the best-fit model to the closed-geometry constant-density scenario. If we make the assumption that $T_d < 150$ K, then equation (3) constrains A_V to values of 300–650. Taking the effects of a power-law density structure into account, then the observed $[\mathrm{O\ I}]^{63\ \mu\mathrm{m}}_{146\ \mu\mathrm{m}}$ can be reproduced with A_V as large as 750. However, if we consider an asymmetric geometry, then the observed $[\mathrm{O\ I}]^{63\ \mu\mathrm{m}}_{146\ \mu\mathrm{m}}$ can be modeled with $A_V < 650$. Therefore, the systematic effects of density structure and asymmetry largely neutralize each other. Given these facts, we feel that our conclusions about the physical properties of the NGC 6334A PDR are fairly robust.

6. CONCLUSIONS

In this paper, we have presented a series of constant-density PDR models of NGC 6334A. Overall, we find the following:

1. We considered both a single-sided, plane-parallel model (i.e., open geometry, such as Orion) and one in which the PDR emitting region is completely surrounded by molecular gas (closed geometry). We find the Orion geometry, in which the PDR emission is beamed away from us, yields an A_V which is incompatible with the 850 μm emission in the region.

2. We find that a closed geometry is able to simultaneously reproduce the observed [O I] and [C II] emission with realistic values of A_V. Optical depth effects decrease the $[\mathrm{O\ I}]^{63\ \mu\mathrm{m}}_{146\ \mu\mathrm{m}}$ ratio with increasing A_V. Our best-fitting model yields $A_V = 650$ mag, $G_0 = 10^{4.8}$, and $n_{\mathrm{H}} = 10^{5.7}$ cm^{-3}, giving the best agreement with observation. In addition, our results agree well with the results of LJT06, in the limit where both [O I] lines become optically thick.

3. Optically selected objects, like the Orion H II region, tend to be viewed face on, the geometry assumed in most PDR calculations. But IR-selected objects may be viewed from any angle and may be embedded within molecular gas. Therefore, modeling IR-selected regions may often require a different geometry than assumed by open-geometry models such as Kaufman et al. (1999).

4. We show the effects of a density law on the best-fitting model are to increase A_V to $\sim$750 mag or to increase the cloud thickness. If the geometry is asymmetric rather than symmetric, A_V is $<$650. Overall, these two effects largely negate each other.

5. Overall, the calculations outlined here should prove useful in studying heavily embedded star formation, which will be observed by *Spitzer*, *Herschel*, the Stratospheric Observatory for Infrared Astronomy (SOFIA), and the Atacama Large Millimeter Array (ALMA) with regularity.

N. P. A. would like to acknowledge Center for Computational Sciences at the University of Kentucky for financial and computational support, along with NSF grant 0094050. N. P. A. and A. P. S. acknowledge support from Spitzer GO-2 program 20220. G. J. F. acknowledges NSF through AST 06-07028 and NASA through NNG 05-GD81G; T. H. T. acknowledges support for this project from NSF grant AST 03-07642. We thank the anonymous referee for a careful reading of this manuscript and her/his many useful comments.

REFERENCES

Abel, N. P. 2006, MNRAS, 368, 1949
Abel, N. P., Ferland, G. J., Shaw, G., & van Hoof, P. A. M. 2005, ApJS, 161, 65
Bakes, E. L. O., & Tielens, A. G. G. M. 1994, ApJ, 427, 822
Baldwin, J. A., Ferland, G. J., Martin, P. G., Corbin, M. R., Cota, S. A., Peterson, S. A., Bradley, & M., & Slettebak, A. 1991, ApJ, 374, 580
Bertoldi, F. & Draine, B. T. 1996, ApJ, 458, 222
Cardelli, J. A., Clayton, G. C., & Mathis, J. S. 1989, ApJ, 345, 245
Carral, P., Kurtz, S. E., Rodríguez, L. F., Menten, K., Cantó, J., & Arceo, R. 2002, AJ, 123, 2574
Cowie, L. L., & Songalia, A. 1986, ARA&A, 24, 499
Crutcher, R. M. 1999, ApJ, 520, 706
de Pree, C. G., Rodriguez, L. F., Dickel, H. R., & Goss, W. M. 1995, ApJ, 447, 220
Doty, S. D., & Neufeld, D. A. 1997, ApJ, 489, 122
Draine, B. T. 1978, ApJS, 36, 595
Draine, B. T., & Lee, H. M. 1984, ApJ, 285, 89
Ferland, G. J., Korista, K. T., Verner, D. A., Ferguson, J. W., Kingdon, J. B., & Verner, E. M. 1998, PASP, 110, 761
Habing, H. J. 1968, Bull. Astron. Inst. Netherlands, 19, 421
Harvey, P. M., Hyland, A. R., & Straw, S. M. 1987, ApJ, 317, 173
Heiles, C. 1994, ApJ, 436, 720
Hollenbach, D. J., & Tielens, A. G. G. M. 1997, ARA&A, 35, 179
Kaufman, M. J., Wolfire, M. G., & Hollenbach, D. J. 2006, ApJ, 644, 283
Kaufman, M. J., Wolfire, M. G., Hollenbach, D. J., & Luhman, M. L. 1999, ApJ, 527, 795
Kraemer, K., E., Jackson, J. M., & Lane, A. P. 1998, ApJ, 509, 931
Kraemer, K., E., Jackson, J. M., Lane, A. P., & Paglione, T. A. D. 2000, ApJ, 542, 946
Kraemer, K., E., Jackson, J. M., Paglione, T. A. D., & Bolatto, A. D. 1997, ApJ, 478, 614
Liseau, R., Justtanont, K., & Tielens, A. G. G. M. 2006, A&A, 446, 561 (LJT06)
Malhotra, S., et al. 2001, ApJ, 561, 766
Mathis, J. S., Rumpl, W., & Nordsieck, K. H. 1977, ApJ, 217, 425
Melnick, G., Gull, G. E., & Harwit, M. 1979, ApJ, 227, L29
Nomura, H., & Millar, T. J. 2004, A&A, 414, 409
Omont, A. 1986, A&A, 164, 159
Osterbrock, D. E., & Ferland, G. J. 2006, Astrophysics of Gaseous Nebulae and Active Galactic Nuclei (2nd. ed.; Sausalito: University Science)
Persi, P., Tapia, M., & Roth, M. 2000, A&A, 357, 1020
Rodríguez, L. F., Canto, J., & Moran, J. M. 1982, ApJ, 255, 103
Russell, R. W., Melnick, G., Gull, G. E., & Harwit, M. 1980, ApJ, 240, L99
Sandell, G. 1999, A&A, 343, 281
Sarma, A. P., Troland, T. H., Roberts, D. A., & Crutcher, R. M. 2000, ApJ, 533, 271
Savage, B. D., Bohlin, R. C., Drake, J. F., & Budich, W. 1977, ApJ, 216, 291
Savage, B. D., & Sembach, K. R. 1996, ARA&A, 34, 279
Stacey, G. J., Smyers, S. D., Kurtz, N. T., & Harwit, M. 1983, ApJ, 265, 7
Tielens, A. G. G. M., & Hollenbach, D. 1985a, ApJ, 291, 722
———. 1985b, ApJ, 291, 747
Vacca, W. D., Garmany, C. D., & Shull, J. M. 1996, ApJ, 460, 914
van der Tak, F. F. S., van Dishoeck, E. F., Evans, N. J., II, & Blake, G. A. 2000, ApJ, 537, 283
Young Owl, R. C., Meixner, M. M., Fong, D., Haas, M. R., Rudolph, A. L., & Tielens, A. G. G. M. 2002, ApJ, 578, 885